Supplementary Materials

S1 Spectra comparison

To check the validity of using the Kaimal et al. (1972) spectrum for the Moore (1986) correction, the 30-minute (co)spectra of w, T, a, $w'T'$ and $w'a'$ are computed, where a is the absolute humidity. The cospectrum $S_{w\chi}(f)$ of time series w' and χ' is defined, like in Van Tiggelen (2023), as the real part of the cross-spectrum with frequency f and describes how the turbulent flux information is distributed in the frequency space:

$$S_{wX}(f) = \mathcal{R}\left[\mathcal{F}_w(f) \cdot \mathcal{F}^*_\chi(f)\right] \tag{S1}$$

Where $\mathcal{F}^*_\chi(f)$ is the complex conjugate of $\mathcal{F}_\chi(f)$, which is the Fourier transform of the signal $\chi'(t)$ and is defined as:

$$\mathcal{F}_\chi(f) = \frac{1}{\sqrt{2}} \int_{-\infty}^{+\infty} \chi'(t) e^{ift} \mathrm{dt}. \tag{S2}$$

Since the spectra are quite sensitive to noise, the period of the 1st to the 6th of June is chosen, which is a period with calm and clearsky conditions. The cospectra are computed using the TK3 working memory, which provides the raw data on which the unit conversion, despiking and cross-correlation correction are already applied. Planar fit correction is applied manually using the planar fit coefficients provided by TK3. The S_{ww}, S_{aa}, S_{TT}, S_{wT}, S_{wa} cospectra and frequencies are then normalized in the following way:

$$\text{Normalized spectrum} = \frac{f S_{xx}(f)}{\overline{x'x'}} \tag{S3a}$$

$$\text{Normalized frequency: } n = \frac{fz}{U} \tag{S3b}$$

In general, only the spectra are used for the intervals that have passed the post-processing criteria (described in Sect 3.1). However, an extra round of filtering is applied to get the cleanest spectra. So the following criteria are added:

- $3\,\mathrm{m\,s^{-1}} < U < 8\,\mathrm{m\,s^{-1}}$
- $\left| \frac{\overline{v'w'}}{\overline{u'w'}} \right| < 0.25$

Where the first point strengthens the windspeed criteria to assure turbulent exchange and the second is a good quality parameter. Two intervals which passed these criteria, but still showed a high amount of noise were manually removed, leaving a total of 109 spectra. Two rounds of averaging are applied over the resulting spectra, first averaging all the spectra based on frequency and then averaging this result over bins ranging from n = 0.01 to n = 6. The S_{ww}, S_{wT} and S_{wa} spectra are also compared to the Kaimal et al. (1972) spectrum. For this, the equations used in TK3 are applied (Mauder and Foken, 2015), which are based on Moore (1986) and Kaimal et al. (1972).

For stable conditions (z/L < 0): For $\overline{w'w'}$:

$$\frac{f \cdot S_{ww}(f)}{\overline{w'w'}} = \frac{n}{A_w + 3.124 \cdot (A_w)^{-2/3} \cdot n^{5/3}} \tag{S4a}$$

$$A_w = 0.838 + 1.172 \cdot \frac{z}{L} \tag{S4b}$$

For $\overline{w'T'}$ and $\overline{w'a'}$:

$$\frac{f \cdot S_{xy}(f)}{u_* \cdot y_*} = \frac{0.88 \frac{n}{n_0}}{1 + 1.5 \cdot \left(\frac{n}{n_0}\right)^{2.1}} \tag{S5a}$$

$$n_{0,wT} = 0.23 \cdot \left(1 + 6.4\frac{z}{L}\right)^{0.75} \tag{S5b}$$

Unstable conditions (z/L $\geq$ 0): For $\overline{w'w'}$:

$$\frac{f \cdot S_w w(f)}{u_*^2} = \frac{2n}{1 + 5.3n^{5/3}} + \frac{32n\zeta}{(1 + 17n)^{5/3}} \tag{S6a}$$

$$\zeta = \left(\frac{z}{-L}\right)^{2/3} \tag{S6b}$$

For $\overline{w'T'}$ and $\overline{w'a'}$:

$$\frac{f \cdot S_{wT}(f)}{\overline{w'T'}} = \begin{cases} \frac{11n}{(1+13.3n)^{1.75}} & n < 1 \\ \frac{4.4n}{(1+3.8n)^{2.4}} & n \geq 1 \end{cases} \tag{S7}$$

The resulting spectra are provided in Figure S1.

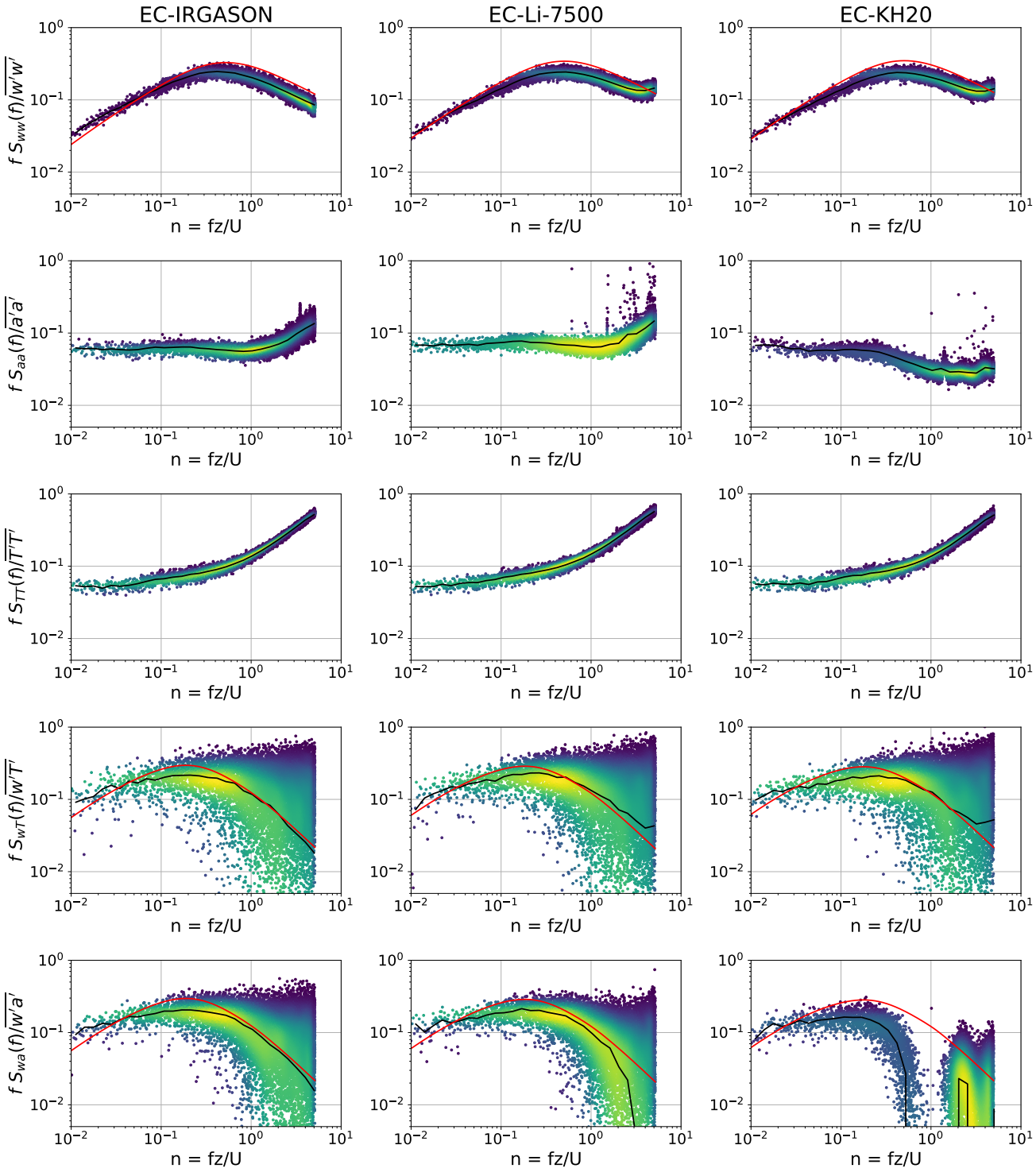

Figure S1. Normalised S_{ww}, S_{TT}, S_{aa}, S_{wT} and S_{wa} spectrum of the EC-IRGASON, EC-Li-7500 and EC-KH20. The dots show the frequency-averaged spectrum, where the colour scale indicates the density of the scatter and increasing brightness corresponds to increasing scatter density. The black line shows the frequency- and bin-averaged spectrum and the red line is the Kaimal spectrum.

S2 Data filtering

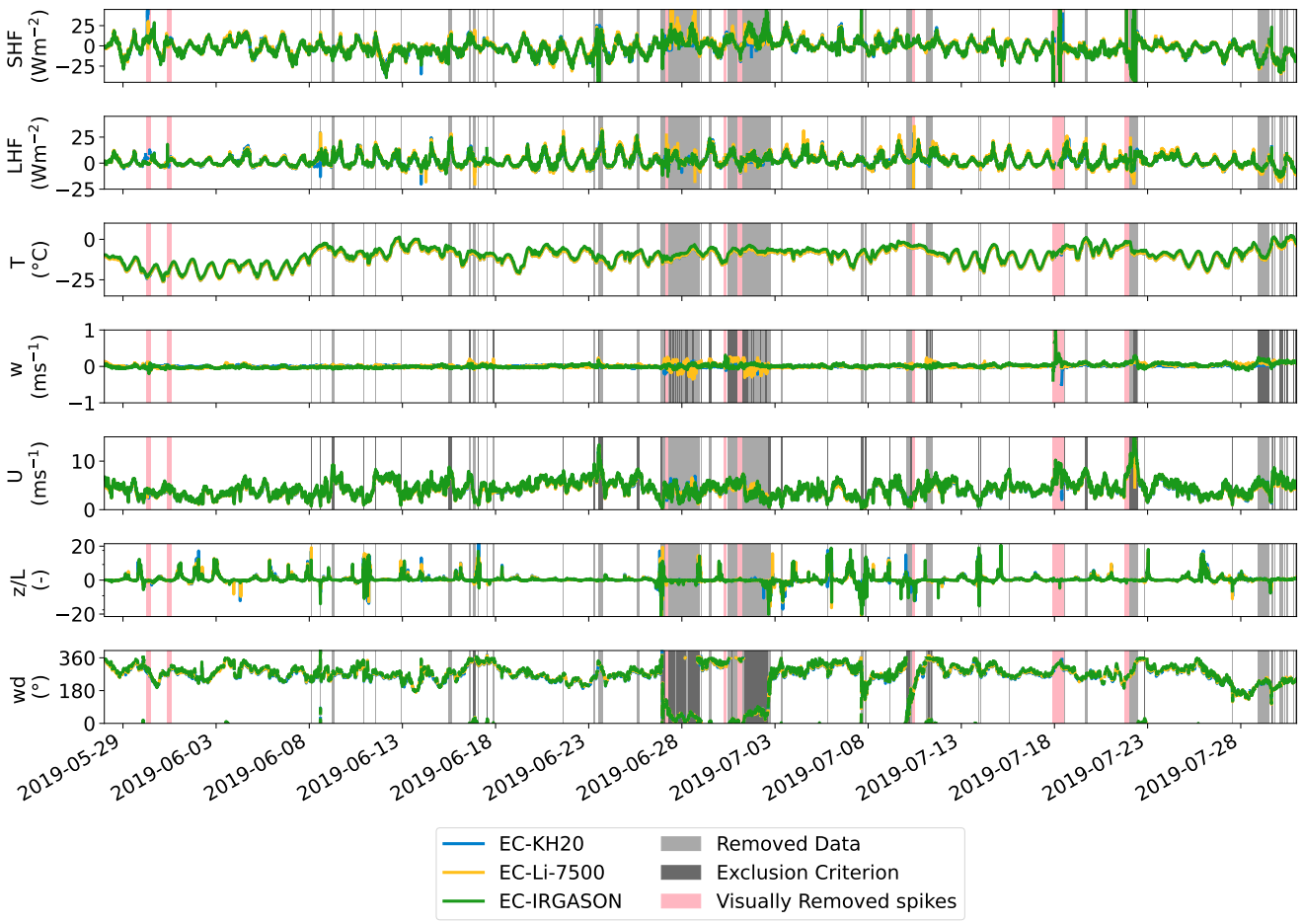

Figure S2. Timeseries of 10-minute averaged EC data after TK3 processing, but before post-processing filtering. In grey, the data removed based on the filtering criteria is shown, where dark grey indicates the variable(s) that did not meet the conditions. In pink, the data that is removed based on the visual inspection is indicated. The stability (z/L) is plotted on a symmetrical log scale, where the part between -1 and 1 is linear and values outside are plotted on a log scale.

S3 Separated slopes

Table S1. Slopes from the data displayed in Fig.5abc, for only positive and negative LHF measured by the EC-IRGASON

Bulk LHF	LHF EC-IRGASON >0	LHF EC-IRGASON <0
PROMICE orig $z_{0,m}$ = $1\mathrm{e}-3\,\mathrm{m}$, $z_{0,q}$ = Smeets and Van den Broeke (2008a, b)	2.09	2.27
PROMICE calc $z_{0,m}$ = $1.3\mathrm{e}-4\,\mathrm{m}$, $z_{0,q}$ = Andreas (1987)	1.36	1.49
PROMICE calc $z_{0,m}$ = $1.3\mathrm{e}-4\,\mathrm{m}$, $z_{0,q}$ = $5.7\mathrm{e}-7\,\mathrm{m}$	0.9	0.98

Table S2. Slopes from the data displayed in Fig.5efg, for only positive and negative SHF measured by the EC-IRGASON

Bulk SHF	SHF EC-IRGASON >0	SHF EC-IRGASON <0
PROMICE orig $z_{0,m}$ = $1\mathrm{e}-3\,\mathrm{m}$, $z_{0,q}$ = Smeets and Van den Broeke (2008a, b)	1.23	1.29
PROMICE calc $z_{0,m}$ = $1.3\mathrm{e}-4\,\mathrm{m}$, $z_{0,q}$ = Andreas (1987)	0.78	0.84
PROMICE calc $z_{0,m}$ = $1.3\mathrm{e}-4\,\mathrm{m}$, $z_{0,q}$ = $2.9\mathrm{e}-4\,\mathrm{m}$	0.87	0.94

S4 Bulk fluxes timeseries

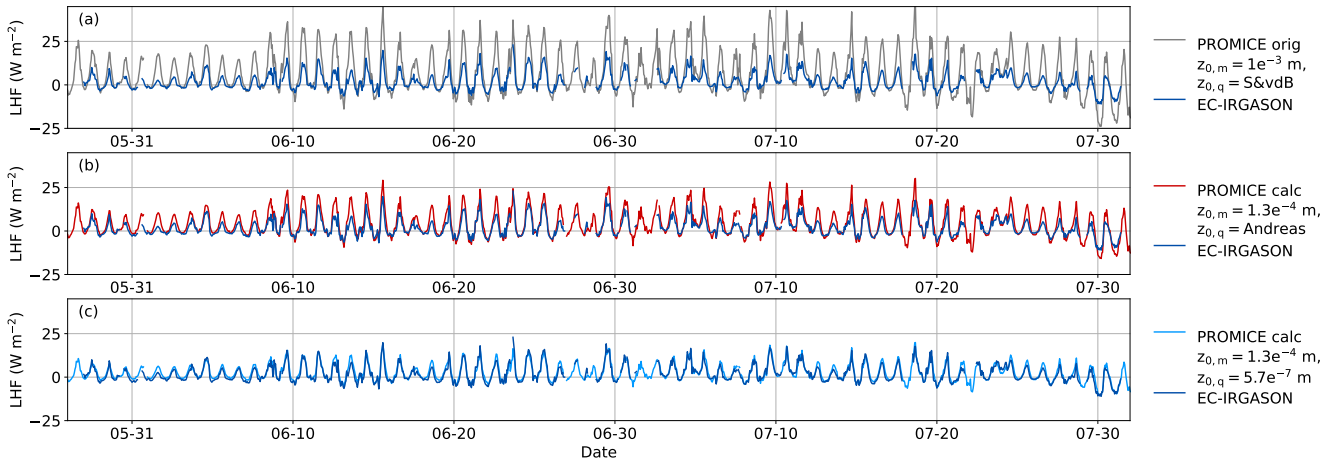

Figure S3. Timeseries of the bulk LHF based on the PROMICE AWS observations and EC-Irgason LHF. Panel (a) is based on the original PROMICE data product using $z_{0,m}$=1 $\times$ 10^{-3} m and $z_{0,q}$=$z_{0,t}$=(Smeets and Van den Broeke, 2008a, b)(S&vdB). Panel (b) is the bulk flux recalculated using the $z_{0,m}$ from the EC-Irgason and parameterizations from Andreas (1987). Panel (c) shows the calculated bulk flux using the $z_{0,m}$, $z_{0,q}$, and $z_{0,t}$ values derived from the EC-Irgason.

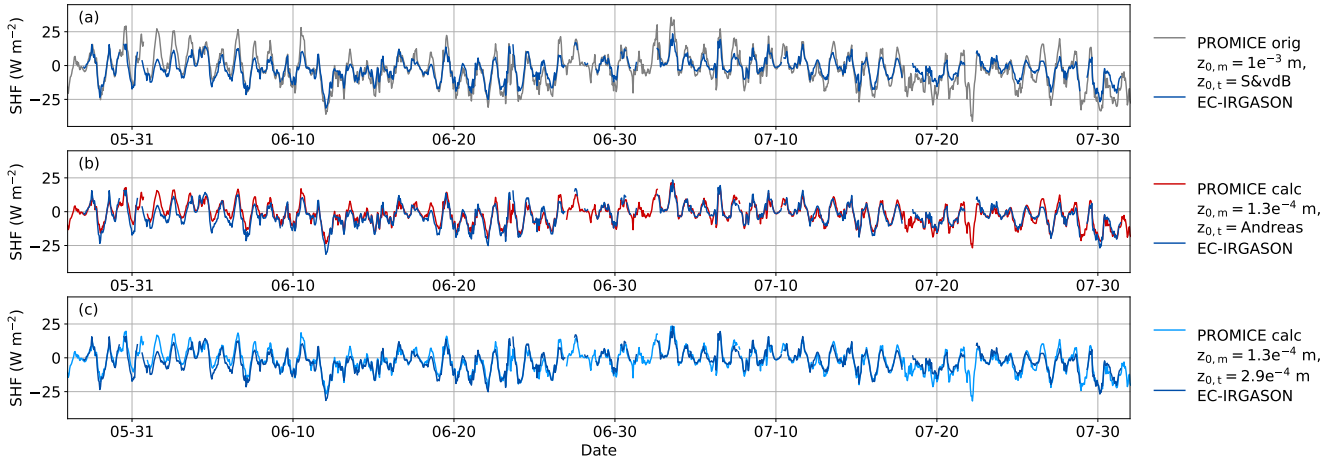

Figure S4. Timeseries of the bulk SHF based on the PROMICE AWS observations and EC-Irgason SHF. Panel (a) is based on the original PROMICE data product using $z_{0,m}$=1 $\times$ 10^{-3} m and $z_{0,q}$=$z_{0,t}$=(Smeets and Van den Broeke, 2008a, b)(S&vdB). Panel (b) is the bulk flux recalculated using the $z_{0,m}$ from the EC-Irgason and parameterizations from Andreas (1987). Panel (c) shows the calculated bulk flux using the $z_{0,m}$, $z_{0,q}$, and $z_{0,t}$ values derived from the EC-Irgason.

S5 PROMICE longwave radiation

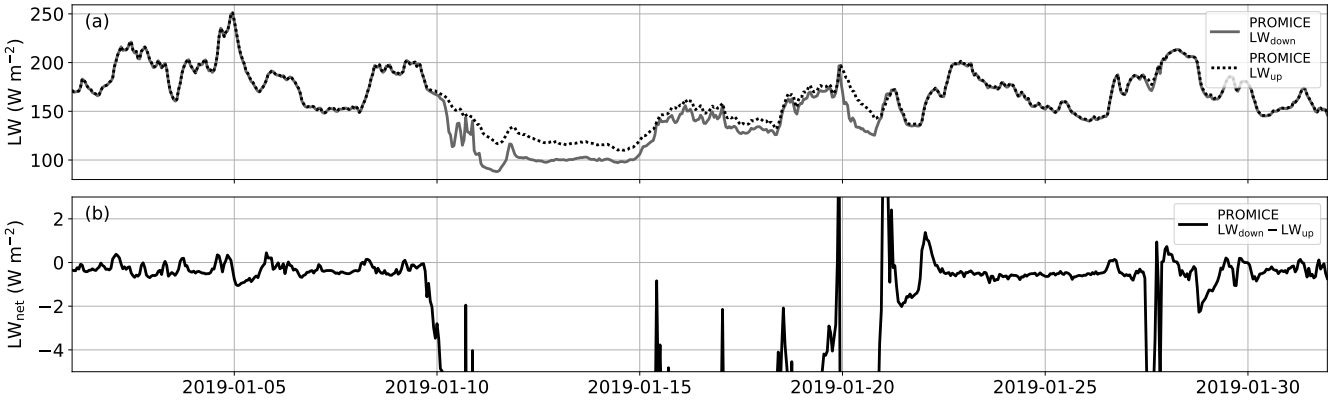

Figure S5. Time series of the PROMICE AWS winter longwave radiation observations with (a) the separate up- and downwards measured longwave radiation and (b) net longwave radiation on a magnified y-axis highlighting variability in the near-zero net radiation.

References

Andreas, E. L.: A theory for the scalar roughness and the scalar transfer coefficients over snow and sea ice, Boundary-Layer Meteorology, 38, 159–184, https://doi.org/10.1007/BF00121562, 1987.

Kaimal, J. C., Wyngaard, J. C., Izumi, Y., and Coté, O. R.: Spectral characteristics of surface-layer turbulence, Quarterly Journal of the Royal Meteorological Society, 98, 563–589, https://doi.org/https://doi.org/10.1002/qj.49709841707, 1972.

Mauder, M. and Foken, T.: Eddy-Covariance Software TK3, https://doi.org/10.5281/zenodo.611345, type: software, 2015.

Moore, C. J.: Frequency response corrections for eddy correlation systems, Boundary-Layer Meteorology, 37, 17–35, https://doi.org/10.1007/BF00122754, 1986.

Smeets, C. J. P. P. and Van den Broeke, M. R.: The Parameterisation of Scalar Transfer over Rough Ice, Boundary-Layer Meteorology, 128, 339–355, https://doi.org/10.1007/s10546-008-9292-z, 2008a.

Smeets, C. J. P. P. and Van den Broeke, M. R.: Temporal and Spatial Variations of the Aerodynamic Roughness Length in the Ablation Zone of the Greenland Ice Sheet, Boundary-Layer Meteorology, 128, 315–338, https://doi.org/10.1007/s10546-008-9291-0, 2008b.

Van Tiggelen, M.: Roughish ice, snow and turbulent heat fluxes on the Greenland ice sheet, https://doi.org/10.33540/1703, 2023.